Natural Resources Canada | Ressources naturelles Canada

GEOMATICS CANADA
OPEN FILE 41

Radar Earth observation methods towards hydrokinetic site selection: a literature review

J.J. van der Sanden and B.J. Nyiri

2018

Canada

GEOMATICS CANADA
OPEN FILE 41

Radar Earth observation methods towards hydrokinetic site selection: a literature review

J.J. van der Sanden[1] and B.J. Nyiri[2]

[1] Canada Centre for Mapping and Earth Observation, Canada Centre for Remote Sensing, 560 Rochester Street, Ottawa, Ontario K1A 0E4
[2] Department of Physics and Astronomy, University of Waterloo, 200 University Avenue West, Waterloo, Ontario N2L 3G1

2018

Permanent address: https://doi.org/10.4095/308412

This publication is available for free download through GEOSCAN (http://geoscan.nrcan.gc.ca/).

Recommended citation
van der Sanden, J.J. and Nyiri, B.J., 2018. Radar Earth observation methods towards hydrokinetic site selection: a literature review; Geomatics Canada, Open File 41, 33 p. https://doi.org/10.4095/308412

Publications in this series have not been edited; they are released as submitted by the author.

Preface

This review was completed under a project funded by the Office of Energy Research and Development of Natural Resources Canada (NRCan). The project entitled “Advancing River Hydrokinetic Energy R&D” is led by the Ottawa Research Centre of NRCan’s CanmetENERGY laboratory and has the participation of NRCan’s Canada Centre for Mapping and Earth Observation (CCMEO), the National Research Council of Canada, the Canadian Hydrokinetic Turbine Testing Centre (CHTTC) of the University of Manitoba, the Laboratoire de Mécanique des Fluides Numérique (LMFN) of Laval University, New Energy Corporation Inc. and Mavi Innovations. Its overall goal is to assess and develop Canada’s river hydrokinetic potential as a national renewable and clean energy source. Hydrokinetic installations may also enhance the resilience of remote northern communities to climate change by reducing their dependence on winter roads to bring in diesel for electricity generation. Specifically, this literature review is meant to provide a starting point for the development of an automated approach to identify candidate hydrokinetic turbine sites in SAR satellite images.

Table of Contents

1 Introduction

This text reviews studies published after 2007, that address the separation of open water from other surface cover types—mainly freshwater ice—by means of Synthetic Aperture Radar (SAR) imagery. The information gained supports a study that aims to evaluate and develop the use of SAR imagery for the selection of river sections suitable for river hydrokinetic turbine installation. In countries, such as Canada, which are marked by large geographic extent, low population density and limited accessibility, the use of any ground-based approach to hydrokinetic site selection would be impractical at best. The usefulness of Earth Observation (EO) satellites towards hydrokinetic site selection is anticipated to derive from a capacity to detect areas of persistent open water in otherwise ice covered rivers. Such open water areas are hypothesized to correspond to high flow rate river reaches, and so EO satellites could be used to identify suitable locations for electricity generation by means of hydrokinetic turbines. Results published by d'Auteuil et al. (2015) corroborate this hypothesis to a certain extent and demonstrate the potential of oblique aerial photographs and optical EO satellite images for the detection of open water in ice covered rivers. Relative to these data sources, SAR satellite images offer an advantage because their information content is not adversely affected by haze, clouds or nighttime darkness. The ability of SAR satellites to capture surface cover information in the absence of solar illumination is a distinct benefit given the darkness of winter in the Canadian North. Indeed, this circumstance has motivated Canadian organizations to assume a leading role in the research and development of radar EO satellite technology and applications. This has led to successful single SAR satellite missions such as RADARSAT-1 (1995-2013) and RADARSAT-2 (2007-to date). The RADARSAT Constellation Mission—a configuration comprised of three SAR satellites—is presently scheduled for launch in the fall of 2018. Readers interested in its specifications are referred Thompson (2015). Studies dealing with optical EO sensors are not reviewed because these sensors cannot be relied upon to image the areas of interest during the winter season. If available, however, high to medium resolution optical EO images typically offer excellent utility for ice-water discrimination.

Publications that specifically address the use of SAR images for the detection of open water on ice covered rivers during the winter season are relatively rare. Therefore, we choose to review how radar data have been used in a variety of comparable applications. Such uses include the delineation of sea ice from water, water from land, water from lake ice, and ground-fast ice from floating ice in individual SAR images, as well as the mapping of water extent through the detection of changes in multi-temporal SAR image data sets. It should be noted that, due to variations in radar observations resulting from differences in, for example, surface cover type and environmental conditions, the findings published in somewhat off topic references may not directly transfer to the targeted application. As an example, radar data types and analysis methods suitable to differentiate sea ice from water may not be optimal for discriminating river ice from water as a difference in salinity causes the radar measurements of sea ice and river ice to vary considerably. Successful application of SAR remote sensing to hydrokinetic site selection will require a robust ability to distinguish between river ice cover and open water as well as adequate spatial resolution to resolve the two cover types over the

typically narrow width of rivers. The latter requirement precludes the use of data collected by radar altimeters, scatterometers and microwave radiometers—sensors operating with spatial resolutions starting at about 25 x 25 km. Accordingly, papers that discuss the utility of these sensor types for the observation of water and/or ice are not reviewed. Given Canada's large geographic extent, the development of a mostly automated approach to operationally identify candidate turbine sites by means of SAR imagery is highly desirable. The literature review summarized in this text was initiated to guide the future research and development required to establish this approach.

Readers unfamiliar with radar EO technology and its application to the mapping of (partially) ice covered rivers are introduced to selected basics in Section 2 of this report. Next, the Sections 3 to 6 describe our literature search and review results partitioned according to the primary SAR image analysis method used. Section 7 summarizes the findings of the literature review by listing the "Lessons Learned".

2 RADAR Earth Observation Basics

"RADAR" is an acronym for RAdio Detection And Ranging. The basic operating principle of radar systems is as follows: a beam of electromagnetic (EM) waves is transmitted, objects in its path reflect the incident waves in many directions, and waves reflected towards the system are received and recorded. In free-space, the approximate sensor to object, or range, distance follows from the EM signal's velocity, equal to the speed of light, and the delay in time between its transmission and reception. The signal recorded is referred to as the radar backscatter and expressed by means of a complex number that captures both its intensity and phase. The intensity is governed by structural and dielectric properties of the object observed while the phase complements the measured time delay, providing more precise information about the range distance. Radar systems used for the purpose of earth observation (EO) operate with microwaves which are EM waves that are about 1 cm to 1 m in length. They can be either imaging or non-imaging. The imaging radar systems usually found onboard EO satellites are Synthetic Aperture Radar (SAR) systems. These systems exploit the forward motion of the platform and incorporate advanced signal recording and processing technology to create a continuous, high resolution and wide swath image from successive side-looking measurements. In contrast, non-imaging systems are limited by their narrow swath, low resolution and, typically, take discontinuous, nadir-looking (aimed directly below the satellite) measurements. Examples of non-imaging radar systems include altimeters and scatterometers. Mounted on satellites, altimeters are primarily used for surface height observations over open oceans, large seas and the ice sheets of Greenland and Antarctica. Similarly, space-borne scatterometers serve mainly to collect wind information over vast bodies of open water. More details regarding the operating principles of radar EO systems can be found in the literature (e.g. Woodhouse, 2006) and on-line such as in the tutorials available at the NRCan Website (Natural Resources Canada, 2017).

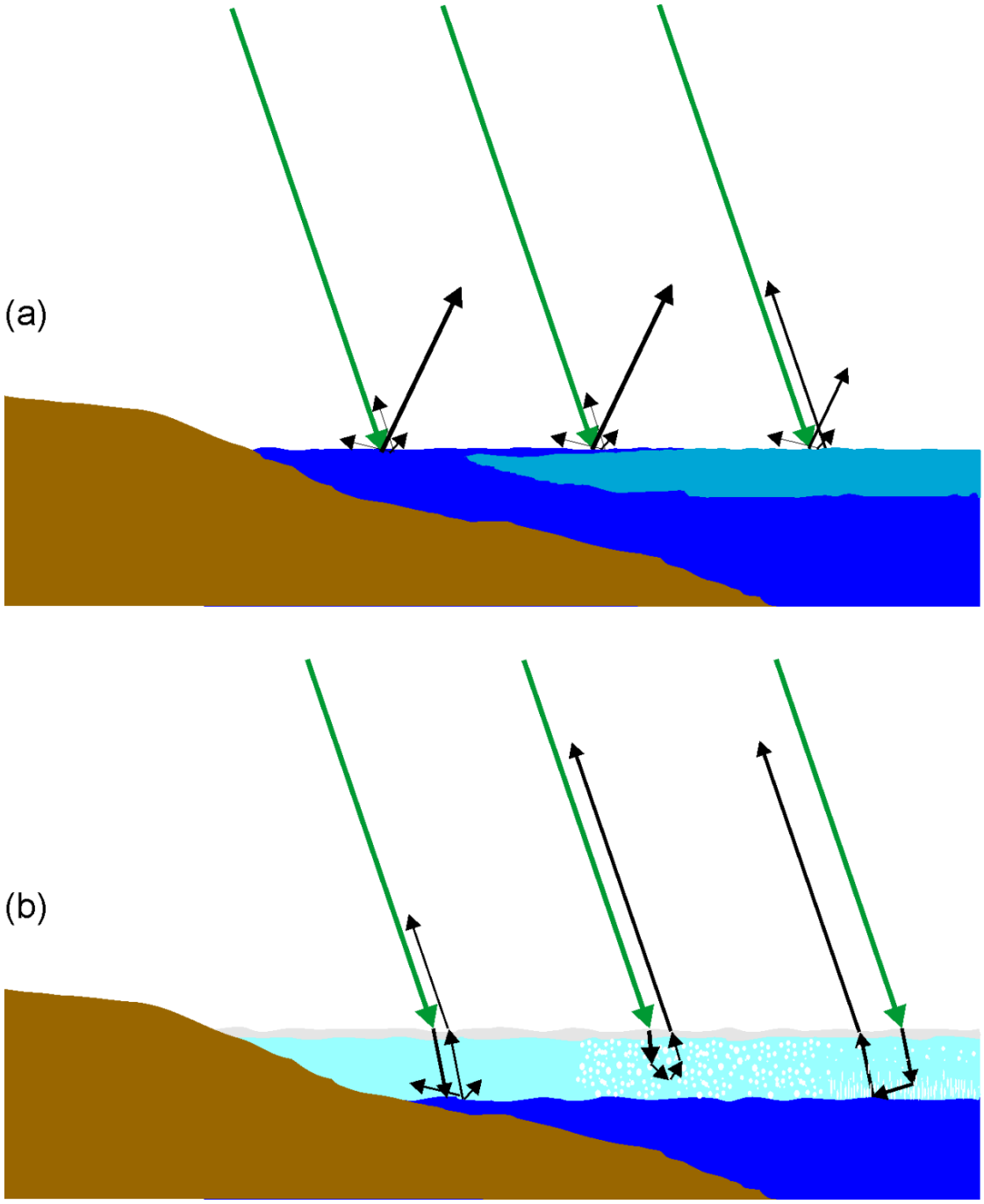

Figure 1 (a-b) Interaction of microwaves with freshwater ice cover and water. The green and black arrows represent incident and transmitted or reflected radar waves respectively; their thicknesses signify the microwaves' intensity. (**a**) surface scattering by (from left to right): open water, water on top of ice and melting ice cover (i.e. ice that includes free water) (**b**) different types of interaction with competent ice cover (from left to right): surface scattering at the ice-water boundary, volume scattering at dielectric discontinuities (e.g. air bubbles), double bounce scattering at—in this case—tubular air bubbles and ice-water boundary.

Generally speaking, the amount of radar backscatter is a function of the scattering properties of the feature observed, sensor characteristics, and viewing geometry. As illustrated in Figure 1, the interaction of microwaves with freshwater ice cover is strongly influenced by the quantity of free water within the ice and any overlying snow. Large amounts of free water promote the reflection of incident waves at the boundary between free-space and the ice cover, i.e. at the snow or ice upper surface (see Figure 1a). In contrast, the absence of free water encourages the penetration of the incident signal into the combined snow/ice volume and subsequent reflection at the ice-water boundary and/or at electrical discontinuities contained within the ice (e.g. air bubbles, cracks, liquid water) (see Figure 1b). It follows, that the backscatter behavior of ice is strongly affected by diurnal and seasonal temperature changes. The dielectric properties of water e.g. open water, water on top of ice or water under ice, prevent microwave penetration and cause incident waves to reflect at its surface.

Reflection of microwaves at boundaries such as those between air and wet ice cover, air and water, or dry ice and water is known as surface scattering. Reflection of the radar signal at multiple discontinuities within the snow and/or ice volume is referred to as volume scattering. A third interaction mechanism known as double bounce scattering involves the reflection of waves at exactly two locations e.g. at an air bubble and the underside of the ice cover. The level of backscatter resulting from surface scattering is governed by the roughness of the surface relative to the wavelength of the incident radar signal. Effectively smooth surfaces will reflect most of the incoming microwaves in the forward direction, that is, away from the radar sensor and therefore create little backscatter (e.g. the water surfaces in Figure 1a). Conversely, effectively rough surfaces will reflect a considerable portion of the incident energy towards the radar and thus generate a substantial amount of backscatter (e.g. ice surface in Figure 1a and ice-water boundary in Figure 1b). Similarly, volume scattering and, especially, double bounce scattering often produce considerable levels of backscatter (see Figure 1b). The scattering behavior of freshwater ice and water can be expected to be most disparate during freezing conditions, making winter the season of choice for the acquisition of radar images in support of hydrokinetic site selection. From an engineering perspective, images collected during late winter, i.e. when the ice cover is fully developed, are preferred because remaining open water areas are likely to have higher than average flows. At all times, low wind conditions are preferred because wind introduces water surface roughness in the form of waves which enhance the water's return signal and heighten the probability of confusion with ice cover.

Sensor characteristics that dominate the radar return signal of features including ice and water are: frequency (or wavelength), polarization, and incidence angle. The wavelength of the radar waves used is important because it (a) affects the depth of penetration in dry ice, (b) defines whether a surface of a given physical roughness is perceived as being 'smooth' or 'rough' by the radar, and (c) defines whether existing discontinuities (e.g. air bubbles) are sufficiently large to contribute to volume or double bounce scattering. Akin to wavelength, incidence angle has an effect on the backscatter level because it influences the penetration depth and sensitivity to physical roughness. Generally speaking, backscatter resulting from surface and double bounce scattering varies more as a function of the incidence angle than backscatter resulting from volume scattering. Polarization affects the backscatter of observed objects

because it defines the plane in which the microwave interaction can occur. For example, microwaves with a horizontal or vertical polarization will only interact with object features in the horizontal or vertical plane respectively. This makes the backscatter behavior of non-spherical scatterers—provided their dimensions are of a scale similar to the incident wavelength—dependent on the incident polarization. As such, polarization diversity provides sensitivity to differences in the structure of the features observed and hence supports their identification. Conventional SAR systems usually acquire backscatter intensity measurements in one or two linear transmit – receive polarization combinations. For example, horizontal – horizontal (HH) and/or horizontal – vertical (HV) or vertical – vertical (VV) and/or vertical – horizontal (VH). In contrast, so-called polarimetric radar systems typically measure the backscatter level in all four mentioned polarization combinations and, in addition, measure the phase difference between the H- and V-polarized receive signals. The received phase information can be used to characterize the observed features' scattering properties in all possible, linear and non-linear, polarization combinations. As such, polarimetric radar images, relative to conventional radar images, often provide more information for target detection and classification. The introduction of radar systems with a capacity to operate in a so-called compact polarimetric mode is a relatively new development. Canada's upcoming RADARSAT Constellation Mission is an example. These systems offer a polarization diversity that falls somewhere between that of conventional and polarimetric radar systems. As such, the information content of images acquired by compact polarimetric systems can also be expected to differ from the information contained in images from either predecessor. The appeal of compact polarimetry, relative to polarimetry, lies in the fact that a single acquisition can provide considerably more coverage. This facilitates the operational application of the data over extended areas.

Finally, the viewing geometry of radar observations, specifically of imaging ones, is important because it defines the orientation of the objects observed relative to the look direction of the radar system. Variations in viewing geometry affect the appearance of features with a directional structure. For example, ice ridges that run in a direction perpendicular to the incident microwaves will show much more clearly than ridges running in other directions. Also, depending on their relative orientation topography and features like river banks, dams, and bridges can induce local image distortions and matching increased or reduced radar return signals. The incidence angle also affects the induction of such distortions. Additional details on the interaction of microwaves with ice cover and water can be found in e.g. Hall (1998), Unterschultz et al. (2009), van der Sanden and Drouin (2011), Duguay et al. (2015) and van der Sanden and Short (2017).

Techniques and methods aimed at discriminating open water from other surface cover types in radar EO images can be labelled image classification approaches. While the information exploited may vary (see sections 3 to 6), two fundamental approaches can be identified. A first group of approaches are ones that involve supervised classification. This type of classification includes the definition of training data units—by means of validation information—that represent classes of interest. These units are then used to extract statistics that quantify the response of each class in the available image channels. Next, the remaining units (e.g. pixels) are assigned to the class with the most similar response. The classification

of one, non-training, unit in no way affects the classification of another. Supervised classification requires the overhead of defining the classes but are robust to outliers and can directly incorporate human understanding. The identification of data for use in training always requires an analyst but the actual training can be done through human intervention or by a variety of pseudo-machine learning techniques such as neural networks, Support Vector Machines (SVMs), and automatic decision tree construction. Besides the aforementioned pseudo-machine learning techniques, decision trees and thresholds—either one- or multi-dimensional—defined by humans represent the most prominent supervised classification methods. A second group of approaches involves the use of unsupervised classification techniques. These techniques have in common that they organize the entire set of data at once by dividing the data into clusters. Algorithms that perform such clustering do not incorporate any pre-existing knowledge about the classes and as a matter of fact do not assign a class to groups identified. The assignment of classes to the clusters is done by an analyst or by what is essentially a supervised classification, for example, the darkest class always being assigned the label of water. So-called K-Means algorithms are by far the most commonly used. For further detail on clustering methods Xu and Wunsch (2005) may be consulted. For detail about supervised methods Kotsiantis (2007) is recommended.

3 Radiometric Analysis

For the purpose of this text, radiometric analysis refers to methods which differentiate surface covers in radar imagery by examining the strength of the radar return signal or “backscatter”. These methods can work well provided the backscatter of the cover of interest is stable over both space and time. Covers that generate high levels of backscatter show in bright tones in SAR images. Features that generate little backscatter show dark. In the case of water and ice, water is often considerably darker than most ice types. However, high wind conditions will increase the backscatter of water and thus complicate ice-water discrimination. Similarly, thermally grown ice cover that is devoid of dielectric discontinuities—black ice or pure columnar ice for short—can be expected to generate little backscatter. Consequently, this type of ice cover is easily misclassified as open water. Ice cover types referred to as snow ice and frazil ice typically produce backscatter levels that exceed those of (calm) water due to the presence of many air bubbles. Readers interested in the definition of ice types and additional ice cover terminology are referred to IAHR (1980). Because water often represents the darkest population of pixels in a given image it is commonly classified using a simple thresholding technique where pixels with values above the maximum value for water are attributed to alternate cover types. This is best done after the application of a filter to remove speckle. Speckle is a multiplicative noise that results from the constructive and destructive interference of the backscattered microwaves. This is a consequence of SAR methods using coherent waves. There are a wide variety of filters in common use. For an overview it is recommended to consult Gagnon and Jouan (1997).

River ice related studies

Van der Sanden et al. (2009) report results of a preliminary study into the information content of C-band, HH-, HV- and VV-polarized images—from RADARSAT-2—relating to river ice freeze-up. The images applied were acquired over the Middle Channel of the Mackenzie River near Inuvik in the period from October 2008 to April 2009. Analysis of the available data shows that the information comprised in HH and VV images is very similar and that the information content of HV images is complementary. Three-polarization color composite products are shown to facilitate the visual detection of initial and complete freeze-up by an image analyst. Relative to the HH and VV images, images acquired in the HV-polarization are shown to offer more utility for differentiating black ice from snow ice and frazil ice. Quantitative analysis of HH, HV and VV backscatter levels reveals a potential for confusion between snow ice and frazil ice and between black ice and bottomfast ice. The latter is relevant for hydrokinetic site selection because of the earlier noted resemblance in the radar return of black ice and open water.

Van der Sanden et al. (2012) introduce a method to classify river ice conditions during spring breakup with the help of C-band, HH-polarized images (e.g. from RADARSAT-1 or RADARSAT-2). Two incidence angle dependent thresholds—starting at 29°—are applied to differentiate between sheet ice, rubble ice and open water. Each ice class is divided in three sub-classes that reflect differences in the ice cover's surface roughness. Thresholding is preceded by two consecutive speckle filtering operations and followed by mode and sieve filtering to reduce heterogeneity in the classified product. Image areas that do not correspond to rivers are masked out by means of ancillary information, i.e. hydrographic vector data. Incidence angles below 36° are found to complicate discrimination between open water—under calm to light breeze wind conditions ($\leq$ 11 km/h)—and sheet ice. Textural analysis is applied with some success to alleviate this problem. Output products have been validated in a qualitative sense by means of oblique aerial photographs. The classes showing in products derived from images that are acquired during freezing conditions, i.e. the winter season, should not be considered accurate because the backscatter behaviors of competent and melting ice differ. In the years following its inception the method has been applied to monitor ice breakup in a series of Canadian rivers. Beaton et al. (2017) discuss the utility and limitations of the approach based on an evaluation of a series of information products as generated for selected rivers in Ontario's Far North during the 2015, 2016 and 2017 breakup seasons.

Łoś et al. (2016) compare the utility of dual polarization (HH, VV) RADARSAT-2 (C-band) and TerraSAR-X (X-band) data for the classification of river ice. The data were acquired over the Peace River, Alberta, Canada at the time of freeze-up (December 2013). Associated incidence angles ranged from 33° to 40° and 23° to 29° for RADARSAT-2 and TerraSAR-X, respectively. Six classes are identified: open water, skim ice (open water mixed with thin columnar ice sheets), juxtaposed skim ice (compilation of thin columnar ice sheets forming a complete cover), agglomerated skim ice (compilation of thin columnar ice sheets overriding each other forming a complete cover), frazil runs (open water mixed with frazil ice rafts and pans), consolidated ice (deformed or ridged ice). All four radar return signals for each class were observed to be very similar, barring some effects hypothesized to result from incidence

angle variability. A supervised maximum-likelihood classifier based on the complex Wishart distribution, preceded by speckle filtering, was used. This classifier makes use of the so-called Covariance Matrix or Coherency Matrix—derivatives of the Sinclair Scattering Matrix—and is typically used for the classification of polarimetric images (Lee et al., 1995). Overall classification accuracies ranged from 81% to 88% and 84% to 99% in the case of TerraSAR-X and RADARSAT-2, respectively. Accurate discrimination between skim ice and open water, juxtaposed skim ice and agglomerated skim ice, and (juxtaposed) skim ice and frazil runs was found to be problematic.

Lake ice related studies

Geldsetzer et al. (2010) present a thresholding approach for discriminating between melting lake ice and open water by means of RADARSAT-2 dual-polarization products, i.e. C-band HH and HV images. The threshold established for each polarization is fixed across the available range of relatively shallow incidence angles (about 34° to 49°). Thresholding is preceded by speckle filtering. The utility of HH-polarized data is observed to be compromised by high wind conditions—causing open water to be misclassified as ice. On the other hand, low return signals from melting ice—causing ice to be misinterpreted as open water—are found to limit the utility of HV-polarized data. Accordingly, HH and HV data are recommended for use during the earlier and later stages of breakup, respectively. By using the HV data at the time that more open water is present the likelihood of misclassifying water as ice is reduced. The decision when to stop using HH and start using HV is left to an image analyst. The backscatter levels of lake ice, in both polarizations, are observed to vary substantially in both space and time. Overall classification accuracies over 81% and ranging from 66% to 97% are reported for the earlier and later breakup stages, respectively.

Sobiech and Dierking (2013) evaluated the utility of K-Means clustering for the classification of melting lake and river ice as well as open water in the Lena River Delta. Classification was always preceded by speckle filtering. A low-pass filter and/or closing filter—designed to remove morphological noise—were applied selectively before and after classification, respectively. In the case of lake ice, the unsupervised clustering results were compared to results achieved by means of a supervised thresholding method. The available radar data set comprised HH-polarized, X-band TerraSAR-X as well as HH-, HV- and VV-polarized, C-band RADARSAT-2 images. Associated incidence angles ranged from about 32° to 40°. Spatial and temporal offsets between the images from the two data sources prevented the direct comparison of the associated results. Ice on/off maps resulting from visual image interpretation were used to assess the accuracy of the automated classification results. With respect to RADARSAT-2, for both lake and river ice, the classification results were found to vary with polarization, i.e. diminishing from HH to HV to VV. Relative to visually produced maps, lake ice classifications achieved by means of automated analysis of TerraSAR-X data yielded average errors in the fraction of ice ranging from 10% to 17%. Similar accuracies were not reported for RADARSAT-2 because the sample was considered too small. Classification using RADARSAT-2 data acquired in more than one polarization was not attempted. In most cases K-Means clustering and thresholding was found to produce comparable results. Easier implementation—because *a priori* knowledge about the scattering behavior of classes (e.g. as a function of incidence angle) is not needed—is mentioned as an advantage of

unsupervised K-Means classification. On the other hand, this clustering approach requires the presence of both ice and water in the image while a supervised thresholding method does not. Selective application of low-pass and/or closing filters yielded mixed results that, surprisingly, differed for lake and river ice.

Sea ice related studies

Geldsetzer and Yackel (2009) present a decision tree approach for the classification of sea ice and open water by means of HH- and VV-polarized, C-band Envisat ASAR data. Images used in the development of the classifier were acquired during the winter season at incidence angles ranging from 26° to 45°. Conventional statistical analysis—as opposed to machine learning—was used to establish a series of thresholds. Thresholds used in the classification of sea ice types (i.e. thin, first-year and multi-year ice) are based on either HH or VV backscatter levels. Thresholds developed to differentiate sea ice from open water make use of VV/HH co-polarization ratios. Application of the classifier reveals limitations in discriminating open water from thin ice at incidence angles below 40° in particular. Results obtained with an image acquired at about 37°, show that open water can be discriminated from thicker ice types with >99% accuracy. However, with the inclusion of thin ice the classification accuracy for water drops to 50%.

Shokr (2009) used daily sea ice charts to determine the C-band HH backscatter of sea ice types and water observed by RADARSAT-1. The charts, produced by the Canadian Ice Service, show polygons that identify areas of a given cover composition (e.g. 2/10 Nilas ice, 2/10 Grey ice, 3/10 first year ice and 3/10 water). This information is used to decompose the mean total backscatter for a given polygon into a linear combination of the mean backscatters for each cover type present. An initial value for the backscatter of component cover types is determined from homogeneous training sites and unequal backscatter contributions—relative to coverage—of cover types of varying brightness are accounted for. The study produced reliable backscatter values for sea ice types as well as open water and facilitated an analysis of the effects of incidence angle and wind speed. An observed increase in the backscatter of seawater with a decrease in incidence angle and under intensifying winds agrees with findings reported in many preceding publications. While not viable as a classification technique, the approach described could theoretically be used to analyze any radar image data where extracting surface cover signatures is complicated by a high degree of heterogeneity.

Flores et al. (2014) combined a novel speckle filtering method with Markov Random Field (MRF) based segmentation to delineate the Antarctic Terra Nova Bay Polynya in a pair of X-band HH COSMO-SkyMed ScanSAR Wide images. MRF segmentation was found to yield a better outline of the polynya than two conventional pixel-based classification approaches—one being unsupervised, the other supervised. Indeed, the approach produced results on par with visual interpretation by an experienced ice analyst. Speckle filtering is highlighted as an essential processing step. A reduction in spatial resolution from 15 x 15 m to 50 x 50 m was found to drastically reduce the efficacy of the MRF approach. Its robustness to backscatter variability introduced by e.g. changing environmental conditions was not tested.

Other studies

Santoro and Wegmüller (2014) use HH- and VV-polarized Envisat ASAR Wide Swath images—acquired in the period from January to December 2015—to map permanent water bodies by means of multi-temporal backscatter intensity metrics, i.e. backscatter minimum and standard deviation. Relative to water pixels, pixels corresponding to land surface types are expected to have a higher minimum backscatter and lower standard deviation. The applied ASAR images are calibrated to sigma naught (in dB), multi-looked to 300 x 300 m pixel size, geocoded to latitude/longitude coordinates and speckle filtered to about 150 equivalent number of looks (ENL). Furthermore, backscatter measurements over sloped terrain were corrected for pixel area and incidence angle deviations. A series of diverse study sites—covering more than 13 million km^2—is used to develop a simple yet robust threshold-based mapping algorithm. Validation of results by means of CORINE land cover data, SRTM Water Bodies data and Google Earth imagery yields overall classification accuracies above 90%—for pure land and water pixels. The accuracy decreased linearly with water fraction when mixed pixels were taken into account. Pixels with less than 10 ASAR observations were not included in the classification and pixels corresponding to slopes ≥10° were automatically classified as land. Defining the 'backscatter minimum' as the backscatter 5^{th} rank or 10^{th} percentile—as opposed to lowest backscatter measured—was found to limit the misclassification of land as water due to the presence of e.g. wet snow or floodwater. Single- and multi-track data sets were found to yield similar classification accuracies but the authors note that differences in observation geometry could have greater impact on classification accuracies obtained for environments with more volume scattering surfaces (e.g. snow, ice, dry sand) or topography. The effect of polarization could not be assessed because the available data were largely acquired in VV.

Cutler et al. (2015) describe a histogram based thresholding approach to distinguish water from other cover types. The authors use two frequencies and a variety of polarizations; single and dual polarized X-band data from COSMO-SkyMed and TerraSAR-X as well as single, dual and quad-polarized C-band RADARSAT-2 data. The reported method has the advantage of being completely automated. Cases where an algorithm has failed to find a reasonable answer are rejected without user intervention. It achieves this by selecting one of four possible thresholds for each image by means of a disparity metric. The thresholds are computed from two distinct histograms using two different methods. Validation against the USGS national hydrography dataset demonstrates that the method works well only when the fraction of pixels covered by water is between 3/10 and 8/10. This is likely because minimizing population disparity assumes a water fraction around 5/10. The HV polarization is concluded to be best for their purposes as it is least affected by bright nearby features like cities. The data set studied did not include images acquired over surface cover types with backscatter levels that approach the return signal of water nor images corresponding to freshwater ice.

4 Polarimetric Analysis

In brief, polarimetric analysis differs from radiometric analysis because it uses information about the phase of two received radar signals with orthogonal—typically H and V—polarizations. Logically, the acquisition of polarimetric SAR data is a prerequisite for the application of polarimetric analysis techniques. The general idea behind polarimetry is that the features observed are more easily identified by means of information that describes their scattering behavior in all possible combinations of transmit and receive polarizations. This information is captured in the so-called Sinclair Scattering Matrix. However, in practice the acquisition of data in more polarizations rarely causes a proportional increase in available information because of dependencies between certain data. As an example, HV and VH polarized data typically contain identical information. Polarimetric data are typically dealt with in their "linear" basis—as a combination of complex HH, HV and VV data. At times, however, they are transformed to the so-called "Pauli" basis—often referred to as Pauli decomposition—which comprises the complex sum of HH and VV, the complex difference of HH and VV, and two times the complex HV. Relative to the linear terms, the Pauli terms offer more insight into scattering behavior. The Pauli terms one to three are dominated by surface, double bounce and volume scattering, respectively (Lee and Pottier, 2009).

Two widely used techniques to analyze polarimetric images acquired over natural features are the Freeman-Durden and Cloude-Pottier decompositions. The Freeman-Durden (FD) decomposition (Freeman and Durden, 1998) assumes that the Sinclair Scattering Matrix of a given pixel can be meaningfully decomposed into the linear sum of three matrices which represent different basic forms of scattering: volume scattering, surface or "Bragg" scattering and double bounce scattering. The results of this decomposition are meant to reveal the dominant form of scattering of the observed surface cover. A similar model based approach to the analysis of scattering behavior is the Yamaguchi decomposition (Yamaguchi et al., 2005).

The Cloude-Pottier (CP) decomposition (Cloude and Pottier, 1997) is based on the Coherency Matrix—a derivative of the Sinclair Scattering Matrix. The eigenvectors and values of this matrix are used to compute three parameters: entropy (H), Anisotropy (A) and Alpha angle (α). These parameters reflect the randomness of the scatter, the relative power of the 2nd and 3rd eigenvector and the dominant form of scattering (volume, surface or double bounce), respectively. Nine partitions of the plane made up by H and α have been determined to associate with certain types of scatterers and are often used in unsupervised classification approaches. The Touzi decomposition (Touzi, 2007) is another example of an eigenvalue-based decomposition.

River ice related studies

Mermoz et al. (2009) compare the usefulness of two supervised and one unsupervised river ice classification approaches: a rule-based hierarchical—or decision tree—classification, a maximum-likelihood Wishart classification and a Fuzzy K-Means classification. The data used were acquired during the winter of 2003 over Saint François River, Quebec, Canada by an

airborne polarimetric radar system operating in C-band. Four classes of interest are identified: open water, thermal (columnar or black) ice, consolidated ice (deformed or ridged ice), and frazil ice. However, in certain classifications the number of classes was reduced to three by combining thermal ice and frazil ice in one class. The hierarchical classifier was based on the co-polarization ratio (VV/HH), the depolarization ratio (HV/(HH+VV)) and the modulus of the complex correlation between HH and VV. Specifically, the co-polarization ratio is used to identify open water, the depolarization ratio to discriminate consolidated ice from thermal ice and frazil ice and the complex correlation to distinguish between thermal ice and frazil ice. Conventional statistical analysis of training data is used to determine an appropriate threshold for each variable used. The Wishart classification is based on the Covariance Matrix or Coherency Matrix—derivatives of the Sinclair Scattering Matrix (Lee et al., 1995). The unsupervised Fuzzy K-Means classification, a non-polarimetric approach, is driven by HH backscatter and Grey Level Co-occurrence textural information (see Section 4). This approach was first presented by Gauthier et al. (2006). Both polarimetric classifications are found to yield better results than the non-polarimetric K-Means approach. As an example, the K-Means classifier failed to identify open water at the location of a rapid. Quantitative evaluation of results obtained with the hierarchical and Wishart classifier—recognizing four classes—shows overall accuracies of 72% and 66% and accuracies specific to open water of 81% and 69%, respectively. In the hierarchical classification open water was confused with frazil ice only, while in the Wishart classification there was confusion with all three ice classes.

Van der Sanden et al. (2011) evaluate the utility of RADARSAT-2 (C-band) polarimetric images for the monitoring of freeze-up in the Mackenzie River at Inuvik, Northwest Territories, Canada. The images were acquired in the period from October 2008 to April 2009 and covered incidence angles ranging from about 21° to 41°. The analysis is based on data extracted for image regions identified with the help of field observations—training areas in essence. The co-polarization ratio (VV/HH) is observed to facilitate discrimination of open water from newly formed ice cover. However, the utility of the ratio decreases once the ice becomes established and exhibits ratios similar to open water. Also, at any given time, the co-polarization ratio for snow covered river bed is much like the ratio for open water, creating a definite possibility for misclassification. Formation of bottom-fast ice over the course of winter is noted to further complicate the classification of open water. A preliminary analysis of the utility of a series of non-polarimetric and polarimetric variables was limited to the classification of ice types, i.e. columnar ice, frazil or snow ice and consolidated ice. Plots showing the backscatter of columnar, frazil and snow ice cover as a function of time suggest a sensitivity of radar to ice thickness growth. However, differences in structure rather than thickness are observed to control the strength of an ice cover's backscatter on any given date. Logically, this complicates the estimation of ice thickness from backscatter.

Lake ice related studies

Geldsetzer and van der Sanden (2013) evaluate the potential of twenty C-band, polarimetric and non-polarimetric variables to distinguish between open water and floating lake ice—less than two months old. The RADARSAT-2 data studied were acquired over the Old Crow Flats, Yukon, Canada during the 2008-2011 freeze-up seasons and cover incidence angles ranging from 18° to 50°. The non-parametric two-sample Kolmogorov-Smirnov statistic is used to

assess the classification utility of each variable in three incidence angle ranges: 18°-29.9°, 30°-39.9° and 40°-50°. Next, regression analysis is carried out to model the effect of the incidence angle on the most useful variables. The results are used to develop a decision tree type classification approach. As a first step, a fixed threshold for a polarimetric variable known as Conformity is implemented to exclude low-quality backscatter measurements, i.e. open water pixels corresponding to low-wind slicks, from the classification. This is followed by classification of a series of representative data sets by means of six—individually applied—variables: HH or VV backscatter, VV/HH or HV/HH or VH/VV backscatter ratio, or Anisotropy. The best performing variables are found to be: either VV backscatter or Anisotropy (at incidence angles less than about 30°) and the VV/HH backscatter ratio (at incidence angles about 30° and over). These recommended variables are shown to yield classification accuracies ranging from 86% to 99% and 80% to 99% for open water and lake ice, respectively. The utility of Anisotropy, unlike that of VV backscatter, is not limited by wind speeds below about 2 m/s.

Van der Sanden and Geldsetzer (2015) present a comparative analysis of the utility of, C-band, fully polarimetric and compact polarimetric data for the classification of melting lake ice and open water. As mentioned in Section 2, the forthcoming RADARSAT Constellation Mission (RCM) will have the capacity to acquire compact polarimetric data in all imaging modes. This includes modes that operate over wide swaths, i.e. modes that provide the large scale coverage preferred by operational users that deal with extensive areas of interest. For this category of users, RADARSAT-2 polarimetric data are of little interest simply because the associated swath is too narrow ($\leq$ 50 km). The study area is the Old Crow Flats, Yukon, Canada. Results achieved with respect to the compact polarimetric data are used to design a decision tree type classifier that accounts for incidence angle effects. Discrimination between breaking ice and open water is based on incidence angle driven thresholds for the following variables: RR/RL at angles $\leq$ 25°, RR at angles > 25° and < 34° and either RH or RV/RH at angles ≥ 34° (pending a fixed threshold for Conformity). Classification is found to be most difficult in the > 25° and < 34° incidence angle range. Application of the classifier to a series of representative images—including ones acquired during challenging wet snow and high wind conditions—yielded accuracies ranging from about 73% to 99% and 61% to 95% for breaking ice and open water, respectively. These results were found to be comparable to accuracies achieved by means of classifiers that utilize full polarimetric variables.

Sea ice related studies

Gill and Yackel (2012) examine the usefulness of various polarimetric variables for classifying wind-roughened open water and smooth/rough/deformed first year sea ice in the Amundsen Gulf, Northwest Territories, Canada. The RADARSAT-2 images used were acquired in May 2008 under -5° to -2° C temperatures and 9 to 16 m/s winds, at incidence angles ranging from 22° to 37°. All images were filtered to reduce speckle. Field observations were used to create two independent sets of observations for the training of classifiers and the validation of classification results, respectively. The following variables were included in the analysis: CP, FD and Touzi decompositions, polarization phase differences and polarization ratios. Their relative utilities were assessed using the means, standard deviations, and probability density

functions for training areas. Next, variables which provided good separation were used in supervised classifications. Individual variables were entered in K-Means classifications [*sic*] and groups of two/three uncorrelated variables in maximum likelihood classifications. Overall accuracies achieved in classifications with one, two and three variables range from 30% to 74%, 72% to 89%, and 75% to 91%, respectively. The associated classification accuracies for open water range from 17% to 93%, 46% to 96%, and 72% and 98%. CP Entropy and Touzi's dominant eigenvalue are shown to be the best choice for single variable classifications, yielding accuracies for water of about 90% and for sea ice between 36% and 65%. CP Entropy and either VV backscatter or FD volume scattering are among the best performing two variable combinations; water accuracies are about 95% and ice accuracies between 64% and 98%. Not surprisingly, the same variables also contribute to several successful three-band classifications. While the statistical significance of observed differences in classification accuracies was not tested, the differences between two and three variable classifications appear minimal as do those between several well performing combinations in each group.

Other studies

Qi et al. (2012) use RADARSAT-2 (C-band) polarimetric data to classify urban surface covers in Guangzhou City, China. Their analysis approach is object-oriented rather than pixel-based. The data are speckle filtered, transformed to the Pauli basis and segmented—using a bottom-up region-merging technique—to obtain objects. Subsequently, an extremely wide range of variables (>1000) is computed for each object. These include but are not limited to the minima, maxima, means, and standard deviations of: 64 parameters produced by 16 different polarimetric decompositions, backscatter intensities, coherency matrix elements, GLCM-based texture measures (see section 5), interferometric parameters and segment shape indicators. Except for the interferometric parameters, all variables were derived from one single RADARSAT-2 image. About 2000 segments were manually assigned to one of seven classes—water, lawn, forest, barren/sparse vegetation, cropland/natural vegetation, banana or urban/built-up—and used to generate a decision tree classifier by means of a pseudo-machine learning algorithm. Application of this classifier yielded an overall accuracy of 87% but water was identified perfectly. Discrimination between water and lawn—comparable to black ice in terms of backscatter level—is based on variables that capture spatial variability. Given that the classifier was developed and tested by means of one single image, the achieved accuracies are likely biased and certainly wind induced variability in the backscatter of water is not accounted for. A Support Vector Machine (SVM) classification algorithm yielded a near-identical overall classification accuracy but on the order of 6% of water objects was misidentified as either lawn or urban area. A supervised Wishart classification—which only uses the coherency matrix elements—produced an overall accuracy of 70%; about 30% of the water objects was misclassified as lawn or barren/sparse vegetation. Applied to individual pixels, the proposed decision tree classifier yielded an overall accuracy of 77% with about 12% of water pixels being misclassified as lawn or barren/sparse vegetation.

Banks et al. (2014) evaluate the utility of RADARSAT-2 (C-band) polarimetric data for the mapping of Arctic shore and near-shore surface cover types including water, substrates and vegetation types. Specifically, the surface cover information comprised in FD and CP

decomposition results is assessed and applied in three unsupervised, Wishart distance-based, maximum-likelihood classifications. In addition, the effect of the SAR incidence angle is evaluated. Polarimetric decomposition and classification are preceded by speckle reduction through application of the Enhanced Lee filter. Relative to other cover types, the scattering behavior of water is observed to vary more as a function of the incidence angle. This agrees with findings published by other researchers. CP-based classifications are shown to yield better results for water than FD-based classifications. The former reveal limitations in discriminating water from, primarily, sandy areas or smooth mudflats whereas the latter confuse water with all other covers studied. Images acquired at medium to shallow incidence angles are found to comprise more useful information and thus offer better classification potential than images acquired at steep incidence angles.

Ullmann et al. (2017) assess the utility of polarimetric RADARSAT-2 (C-band) and ALOS-2 (L-band) data as well as of complex, dual-polarization TerraSAR-X (X-band) and ALOS-1 (L-band) data for the mapping of arctic surface covers including water and different types of tundra vegetation, bare ground and wetland. All data are converted to the Kennaugh Matrix format—a derivative of the Sinclair Scattering Matrix. Image speckle is reduced by means of a moving window averaging filter. The authors do not classify the available images but rather evaluate the classification potential of derived variables by means of—pairwise—class separability measures, i.e. Transformed Divergence and Jeffereys Matusita Distance [*sic*] (Richards, 1993). There is no indication in the paper that the authors checked if their data are normally distributed—a precondition for using these separability measures. The evaluation of class separability is preceded by a statistical analysis of the scattering properties of the classes of interest. The variables considered include: backscatter intensities, Kennaugh Matrix elements and CP, FD and Yamaguchi decomposition parameters. This analysis included an assessment of correlation which, as expected, shows that many of the variables considered are moderately to highly correlated. Generally speaking, the correlations are higher in L-band than in C-band. The correlation between variables related to water was not assessed. A series of box- and scatterplots signify a risk of confusion in both C- and L-band, between water and sand, in particular. Relative to the decomposition parameters, the Kennaugh Matrix elements relating to backscatter intensities and the HH-VV phase difference are concluded to offer better overall class separability. Regardless the wavelength, the CP parameters offered the lowest class separability both for water and overall. Compared to other classes, water is more easily identified but scattering variability introduced by changes in wind speed and direction is not taken into account. Similarly, the effects of differences in incidence angle are not considered.

5 Texture Analysis

In this review, texture is understood to be image texture and is defined as the pattern of spatial distributions of grey tone (Haralick and Bryant, 1976). This type of texture, while not unrelated, should not be confused with the texture or roughness of the observed surface cover. In addition to the spatial and structural properties of the observed feature, the textural information content of a given image is a function of its spatial resolution, radiometric resolution, operating frequency and, in the case of SAR imagery, the operating polarization. Texture analysis is often done by computing various statistical properties from what is known as the Grey Level Co-occurrence Matrix (GLCM). For a good overview of what kinds of statistics may be calculated please refer to Baraldi and Parmiggiani (1995). The GLCM for a given area captures how often certain combinations of pixel grey levels occur at a given offset, i.e. displacement length and direction. In most cases, GLCM textural analysis is carried out by means of relatively small spatial window that moves across the image from pixel to pixel. The efficacy of GLCM textural analysis is affected by the: moving window dimensions, displacement length and direction, statistical property of choice and number of image grey levels. Alternative textural analysis techniques exist but were not used in the literature reviewed with the exception of a method that simply involves the computation of the local grey level variance.

River ice related studies

Gauthier et al. (2008) describe an automated system, named FRAZIL, to map river ice cover characteristics by means of HH-polarized RADARSAT-1 data. FRAZIL combines geospatial analysis and SAR image processing techniques and is designed primarily to inform hydraulic modelling for flood forecasting. The GIS component is used to characterize the geometry of the river channel, while the image processing component yields an ice cover map—with ice jams being the main class of interest. FRAZIL is intended for use during both freeze-up and breakup. The paper includes few details concerning the image processing approach, a better description is provided in Gauthier et al. (2010). The approach can be categorized as a pixel-based three-step unsupervised Fuzzy K-Means classification that uses both textural and backscatter intensity information. The first classification step exploits a GLCM related textural measure—somewhat ambiguously identified as ‘Mean texture’—to generate seven clusters. Subsequent classifications refine the two clusters representing the finest and coarsest textures measured. The cluster representing the finest texture is determined to comprise two classes, i.e. water and a mixture of water and floating ice pans. These two classes are discriminated using information comprised in three GLCM textural measures, i.e. Mean, Homogeneity, Entropy. Details with respect to the adopted window size, displacement length, displacement direction and number of grey levels are lacking. The cluster representing the coarsest texture is determined to consist of moderately and heavily consolidated ice. The HH-polarized backscatter intensity is used to separate these two classes. In Gauthier et al. (2010) certain classes are merged to produce ice maps with a simplified, six class, legend that includes open water. Using ground photographs, the overall accuracy of example maps is estimated to range from 57% to 83% to 100% during breakup, freeze-up and midwinter, respectively. The development of season-specific processing approaches is suggested as a

means to achieve improved classification accuracies during freeze-up and breakup by accounting for high wind and wet snow effects.

Chu et al. (2015) apply HH- and HV-polarized RADARSAT-2 data to the mapping of ice cover conditions—during freeze-up—in the Slave River, Northwest Territories, Canada. The authors use HH and HV backscatter as well as a measure of the temporal change in the HH backscatter (coefficient of variation) in a two-step unsupervised Fuzzy K-Means classification approach. Application of six GLCM texture statistics was considered but they were found to be of limited use. Unfortunately, the paper is short on details regarding the attempted GLCM textural analysis. The initial classification step uses the HH and HV backscatter as input and results in ten clusters that represent four classes. i.e. water, thermal (or black) ice, juxtaposed ice, and consolidated ice. Ground reference information was used to determine that the cluster corresponding to the lowest observed backscatter values comprises a mixture of water and thermal ice. In the second classification step these two classes are discriminated based on information contained in the coefficient of variation—relative to thermal ice areas, areas corresponding to (flood) water display more temporal change. The classification results were validated, qualitatively, by means of aerial and time-lapse photographs.

A paper by Chu and Lindenschmidt (2016) builds on the work reported in Chu et al. (2015). Once again, RADARSAT-2 data is used to characterize ice cover in the Slave River. However, the images were acquired during breakup rather than freeze-up and are mostly of a higher resolution (ultrafine as opposed to fine) and limited to the HH-polarization. The classification approach is modified accordingly. First, the HH backscatter is used to create 10 clusters that represent four classes, i.e. water, intact (sheet) ice, smooth rubble ice and rough rubble ice. Next, water is discriminated from smooth sheet ice by means of GLCM textural statistics—the details are missing. The overall classification accuracies achieved for four different dates range from 67% to 84%; misclassification of sheet ice as water is more common (14% to 42%) than misclassification of water as sheet ice (9% to 21%). The HH backscatter was normalized—to 30°—to limit the effect of incidence angle variability on classification accuracy. However, the authors note that the accuracies of classifications obtained with images ranging in incidence angles from 31° to 49° varied widely. Aside from incidence angle, other possible sensor and terrain related influences on classification accuracy are discussed.

Sea ice related studies

Multiple papers describe the ongoing development of a software package—named MAGIC, MAp-Guided Ice Classification system—that is designed primarily to classify sea ice by means of C-band RADARSAT-1/2 images (e.g. Clausi et al., 2010; Leigh et al., 2014; Ochilov and Clausi, 2012; Yu et al., 2012a; Yu et al., 2012b). As reflected in the name, the software makes use of pre-existing sea ice charts that are produced manually, from RADARSAT images, by analysts from the Canadian Ice Service (CIS). The role of these ice charts has changed as the software evolved. In the earlier versions of MAGIC, the charts are used to restrain an image segmentation process and to manually assign an ice type or water class to each segmented region. In later versions of the software, segmentation is fully automated and the charts are used only to train a Support Vector Machine (SVM) classifier. The 2014 version of MAGIC is described in detail in Leigh et al. (2014). HH- and HV-polarized RADARSAT-2

ScanSAR Wide images are used as input and the output is a map that shows two classes, i.e. sea ice and water. Image areas corresponding to land are identified and excluded from the processing by means of vector shoreline data. To limit the overall processing time, MAGIC first reduces the input data volume through 4 x 4 block averaging—resulting in pixels 200 x 200 m in size. The software incorporates two independent and complementary classification processes and combines the results to produce one single sea ice extent map. The first process involves the segmentation of the HV backscatter intensity image and the unsupervised assignment of one of six preliminary classes to each segment. Compared to the HH image, the HV image varies less with incidence angle—ranging from 20° to 49°. The second process consists of a pixel-based, SVM classifier—previously trained using ice charts—that exploits a series of backscatter intensity and GLCM texture statistics extracted from either the HH- or HV-polarized image. The following GLCM statistics were used in the classification: Mean, Correlation, Dissimilarity, Applied Second Moment [*sic*], Contrast and Standard Deviation. Relative to the HV image, the HH image is found to contain more textural information. The textural statistics were calculated using window sizes ranging from 5 x 5 to 101 x 101 pixels and displacement lengths varying from 1 to 20 pixels in four directions. The paper does not specify the number of grey levels utilized. In contrast to the first process, the SVM classifier assigns one of two final classes to each pixel, i.e. sea ice or water. The GLCM texture statistics are noted to proficiently differentiate between sea ice and water. Finally, the preliminary classes for each segment created in step one are reclassified to sea ice or water by means of the results of the SVM classification. Relative to the pixel-based SVM classification result, the final segment- or region-based result contains less noise and better defined ice-water boundaries. Tested on 20 images acquired over the Beaufort Sea from April to December 2010—thus considering all seasons—the resulting sea ice extent maps agreed with manually produced sea ice charts to a degree ranging from 89.95% to 99.99%—96.42% on average. MAGIC is shown to be robust to variability introduced by changing incidence angles and wind speeds. However, its utility for the mapping of thin/new/grease ice and small ice floes is noted to be limited.

Zakhvatkina et al. (2013) compare the efficacy of a Bayesian and neural network (NN) classification algorithm for the mapping of sea ice in the Central Arctic—during the winter season—by means of HH-polarized Envisat ASAR Wide Swath data. The former classifier uses backscatter intensity, i.e. sigma naught in dB normalized to 25° to alleviate variability across the 17° to 42° image incidence angle range. Speckle is reduced by means of a 4 x 4 block averaging filter. In contrast to a maximum likelihood classifier, a Bayesian classifier requires information concerning the *a priori* probability of the classes considered. On the other hand, the NN classifier uses a variety of GLCM textural statistics in addition to backscatter intensity. The following GLCM statistics were used: Energy, Correlation, Inertia, Homogeneity, Entropy, Cluster Prominence, 3rd Central Moment and 4th Central Moment. The textural statistics were calculated using a window size of 32 x 32 pixels, displacements ranging from 2 to 16 pixels in four directions, and 16 grey levels. The classifiers were trained and evaluated with the help of 12 ASAR images and associated ice charts produced by expert analysts through visual interpretation. The optimal NN topology was selected by evaluating the performance of more than 50 possible NNs. Four classes of interest were identified: open

water/new ice mix, level first-year ice, deformed first year-ice and multiyear ice. However, initial NN classification results revealed substantial misinterpretation of open water/new ice as level first-year ice and for that reason the former class was excluded from further study. Sea ice analysts are noted to separate between these two classes by means of information contained in non-SAR image sources. Tested on 20 images—not used for training—the NN classifier produced average correspondences with ice charts to a degree of 85%, 83% and 80% for level first-year ice, deformed first year-ice and multiyear ice, respectively. In two selected images, level first-year ice, deformed first year-ice and multiyear ice were identified with accuracies ranging from 62.08% to 86.18%, 73.29% to 73.49% and 64.76% to 72.15% by the NN classifier. The corresponding accuracies achieved with the Bayesian classifier were: 73.14% to 94.36%, 24.89% to 55.90% and 52.38% to 67.96%. Relative to the NN classifier, the Bayesian classifier can be implemented on higher resolution images thus enabling the detection of small-scale features but also producing a noisier result. The relatively good performance of the much simpler Bayesian classifier is explained from the large difference in the *a priori* probability for multiyear ice versus level first-year ice and deformed first year-ice, i.e. 0.9, 0.05 and 0.05, respectively. In areas with more variable sea ice characteristics, the Bayesian approach is not likely to work as well. Logically, the need for *a priori* knowledge about class fractions limits the utility of the approach.

In a follow on paper, the Bayesian and NN classifiers discussed above are replaced by a Support Vector Machine (SVM) classifier (Zakhvatkina et al., 2017). Furthermore, HH- and HV-polarized RADARSAT-2 ScanSAR Wide images are applied rather than HH-polarized Envisat ASAR Wide Swath images. The classifier is trained using backscatter and GLCM textural statistics derived from 24 images acquired during the winter season over the Central Arctic. Operational sea ice charts are applied to identify training areas for six classes: new ice/first-year ice/multiyear ice, landfast ice, water/broken ice mix, water/new ice mix, water under high winds, and water under very high winds. However, in the final map product the first three are merged to form one single ‘sea ice’ class while the latter three are merged and labelled as ‘water’. The HH backscatter intensities are normalized to an incidence angle of 35°—using one single linear relationship obtained for pack ice but applied uniformly across each image. Noise floor variations visible in the HV images are reduced through subtraction of Noise-Equivalent-Sigma-Zero (NESZ) values available from header files. The optimal GLCM computational settings and statistics are determined through visual comparison of textural products with ice charts and the analysis of graphs. The thus selected settings are: 64 x 64 pixels window size, 8 pixels displacement in four directions, 32 grey levels and a window step size of 16 pixels. Typical GLCM implementations use a 1 pixel step size in both the x- and y-direction; the paper does not mention whether the adopted step size is applied in both directions or how GLCM statistics are computed for skipped pixels. The following textural statistics were used: Energy, Inertia, Cluster Prominence, Entropy and 3rd Statistical Moment for the HH image and Energy, Correlation, Homogeneity and Entropy for the HV image. HH and HV mean backscatter intensities and corresponding standard deviations were also computed using a 64 x 64 pixels moving window and—presumably—a 16 pixels step size. The performance of the classifier was tested by means of 2705 images acquired in the period January 2013 to October 2015, i.e. covering all seasons. Validation of all results by means of

ice charts revealed an average overall accuracy of 91 ± 4%. Maps derived from images acquired during the summer months are found to be less accurate. This is hardly surprising because (a) the classifier was trained by means of winter images and (b) summer melt reduces the ice-water backscatter and textural contrast. Irrespective the season, there is a high likelihood of confusion between landfast ice and water. Reliable assessment of classification/mapping accuracy is noted to be complicated by the coarse spatial resolution of operational sea ice charts.

6 Coherent Change Detection

Coherent change detection is an interferometric SAR (InSAR) analysis technique. InSAR involves the acquisition and processing of two compatible radar data sets to obtain information for mapping purposes (e.g. Rosen et al., 2000, Woodhouse, 2006, Moreira et al., 2013). Two forms of information are gained: coherence and phase difference. The coherence ranges from 0 to 1 and signifies the correlation between the radar measurements and the quality of their phase difference. High coherence indicates strong correlations and meaningful phase differences, while low coherence denotes the opposite. The correlation between successive images varies due to changes in the SAR system and the surface observed. Typically the phase differences are the sought-after information because they enable the mapping of e.g. topography and subsidence. Nevertheless, thanks to its sensitivity to surface change, coherence can be used to classify and map surface cover types. Its utility to distinguish between certain cover types depends strongly on their rate of change and the timing of the image acquisitions. Previously, satellite InSAR image pairs could only be acquired with time offsets ranging from days to weeks. To date, much shorter repeat imaging intervals are available from the German TanDEM-X mission—milliseconds to seconds (Krieger et al., 2013).

Lake ice related studies

Van der Sanden et al. (2018) evaluate and develop the utility of InSAR coherence computed from HH-polarized TanDEM-X image pairs, acquired at intervals of about 0 and 10 seconds, for the mapping of lake ice extent during freeze-up. Coherence computed from images acquired 10-seconds apart is shown to facilitate reliable classification of water and lake ice—with the exception of ice ≤ 5 days in age. A simple, automated mapping approach is described and demonstrated. The approach combines basic interferometric processing, ice-water classification using a 0.3 coherence threshold and geospatial analysis to separate lakes from land. Its success primarily derives from the presence and absence of temporal change—resulting in low and high coherence—in the case of water and ice, respectively. Relative to backscatter intensity, InSAR coherence is concluded to offer more utility for lake ice extent mapping because ice and water can be discriminated under all wind conditions and largely independent of the incidence angle. TanDEM-X images acquired at intervals close to zero seconds do not facilitate ice-water classification because water will only loose coherence after about 10 milliseconds (Bamler and Hartl, 1998). At present, TanDEM-X is the only civilian

satellite system with a capacity to acquire images with time offsets on the order of seconds, i.e. intervals ideally suited to ice-water discrimination. Unfortunately, this capacity is not routinely used and thus not available for operational lake ice extent mapping or hydrokinetic site selection. Canada's RADARSAT Constellation Mission (RCM)—scheduled for launch in October 2018—will have the capacity to acquire InSAR image pairs with a 4-day time delay (Thompson, 2015). In order for RCM data to be of use for coherent change detection in the context of hydrokinetic site selection, the ice cover observed will have to maintain sufficient coherence and thus experience limited temporal change—water will naturally lose coherence as desired. Lake and river ice coherence products shown in van der Sanden et al. (2013)—derived from COSMO-Skymed images (X-band, HH-polarized) acquired 4-days apart during mid-winter—suggest that this may be the case. However, analysis of actual RCM data will be required to confirm its utility.

Sea ice related studies

Yitayew et al. (2017) apply HH-polarized TanDEM-X image pairs, acquired with 30 millisecond and 10 second time separations, to the mapping of sea ice. The authors use Relative Kurtosis (a measure of texture), backscatter intensity and InSAR coherence as inputs for an unsupervised clustering algorithm. Following an evaluation of initial results, Relative Kurtosis is dropped because it provides insufficient separation between the classes of interest. Relative to backscatter intensity, InSAR coherence is found to be a more reliable source of information for the identification of unsteady classes, i.e. leads, open water and new ice. On the other hand, backscatter intensity is observed to better support the classification of steady classes such as landfast ice, ice ridges, first- and multi-year sea ice. Both data sets are concluded to have time separations suitable for the detection of water and other unsteady features. In contrast to 10-second repeat TanDEM-X data, 30-millisecond repeat data are available from an operational TanDEM-X mode, i.e. the Alternating Bistatic cooperative mode.

Other studies

Wendleder et al. (2013) describe an approach to generate a "Water Indication Mask" from HH-polarized TanDEM-X bistatic image pairs—acquired at intervals ranging from 50 milliseconds at the equator to 0 milliseconds at the Earth's poles. The mask is meant to be used in the editing of TanDEM-X digital elevation model (DEM) products, i.e. the 'flattening' of areas corresponding to water. A minimum of three image pairs—separated in time by months to years—is used to determine the likelihood that a given pixel corresponds to water. The detection of water in each of these image pairs is based on thresholds for backscatter intensity and InSAR coherence. In fact, two backscatter thresholds are used (-18 dB, -15 dB) to account for calm as well as high wind conditions. An analysis of 1700 globally distributed and randomly selected TanDEM-X products shows that the coherence for water ranges from about 0 to 0.3. To limit potential confusion between water and, in particular, forested areas the authors adopt a coherence threshold value of 0.23. Prior to thresholding, a 5 x 5 median filter is applied to reduce noise in both the amplitude and the coherence images. The window size used to compute coherence is not mentioned. Deserts and ice covered regions as well as areas corresponding to radar shadow or slopes > 20° are excluded from the processing. Also, detected water bodies and islands smaller than, respectively, 2 ha and 1 ha are discarded. "Water Body Detection Masks" (WBDs) generated from each available image pair

are combined to create one single “Water Indication Mask” (WAM). The pixels in the WAM represent water detection ‘counts’ for each threshold across all three dates. Logically, a higher count signifies a higher likelihood that water is present. Relative to the WBDs, the WAM is less sensitive erroneous detections. Validation of mapping results by means of reference data reveals that backscatter intensity facilitates superior detection of fine details such as narrow rivers while coherence provides better separation between water and other low backscatter features including wet or snow covered fields. The authors conclude “dependent on climate, land cover or application, the amplitude and/or coherence derived water body detection mask must be chosen in order to achieve the best classification for accurate water body detection”. For example, coherence thresholding was found to produce poor results when applied to data acquired while water bodies are covered by ice and attain landlike coherences. Excluding such conditions, overall water detection accuracies ranging—across latitudinal zones—from about 51% to 72% are achieved. The corresponding errors of omission range from about 14% to 30%. Close to the Earth’s poles TanDEM-X bistatic images are acquired within less than 10 milliseconds, i.e. the minimum time needed for water to loose coherence (Bamler and Hartl, 1998). Accordingly, the detection results achieved in these regions will be less accurate.

7 Lessons Learned

This text reviews 34 publications regarding the use of Synthetic Aperture Radar (SAR) data in the mapping of river ice, lake ice, sea ice and/or water. Only seven apply SAR images to detect river ice and water in the period starting at freeze-up and extending into winter—features and seasons of interest for hydrokinetic site selection (Chu et al., 2015; Gauthier et al., 2006/2008/2010, Mermoz et al., 2009; van der Sanden et al., 2009/2011). This text also includes supporting references, e.g. to publications outlining relevant image analysis techniques.

Reflecting on the literature it is apparent that:

- C- and X-band SAR images are most commonly used and offer similar utility in support of ice cover and/or water mapping.
- Persistent freezing conditions enhance the utility of C- and X-band SAR images for the detection of open water in ice covered rivers.
- HH- and VV-polarized SAR images typically comprise similar ice/water information while the information contained in HV-polarized images is complementary.
- Four principal SAR image analysis approaches may be identified: radiometric analysis, polarimetric analysis, texture analysis and coherent change detection.
- Preexisting geospatial information such as vector data outlining rivers, lakes and shorelines is often used to constrain image processing and facilitate map production.
- Speckle filtering is essential to achieve good ice/water classification by means of radiometric and polarimetric analysis approaches.
- The changing backscattering behavior of water—due to wind and/or flow—typically hampers and occasionally facilitates its detection.
- Mapping approaches that exploit the variable nature of water involve the detection of temporal change with a minimum of two SAR images by computing backscatter variability or interferometric coherence—the radar return signal of the other surface covers imaged (e.g. ice) must be relatively stable.
- Incidence angle induced changes in the backscatter of water and ice need to be accounted for to achieve consistent mapping results with SAR images acquired in different beams.
- The optimum incidence angle for ice/water classification varies as a function of the image analysis approach.
- Relative to conventional SAR image data, polarimetric and compact polarimetric SAR data offer enhanced opportunities for ice/water classification.
- The Grey Level Co-occurrence Matrix (GLCM) technique is the most commonly used textural analysis approach.
- Texture analysis is widely and successfully used in sea ice mapping approaches, its utility for river/lake ice mapping is less often explored but appears variable.
- Relative to radiometric, polarimetric and textural analysis approaches, the coherent change detection approach is less sensitive to the complicating effects wind and

incidence angle on the classification of water and ice—the timing of the required interferometric SAR acquisitions is critical.

- The majority of supervised classification approaches use either single measurement thresholds, multi-measurement thresholds (i.e. decision trees) or Support Vector Machines.
- The majority of unsupervised classification approaches use (Fuzzy) K-Means clustering.
- The linking of measurements to surface covers of interest resides with the developer and end user in the case of supervised and unsupervised classification approaches, respectively—the absence of certain cover types complicates the interpretation of unsupervised classification results.
- Segment- or region-based approaches yield more homogeneous and better delineated ice/water classes than pixel-based approaches—demonstrated for sea ice mapping.
- Pixel-based ice/water classification approaches dominate the literature because automated segmentation of SAR images showing natural surface covers is very challenging.
- Radiometric analysis approaches are likely to confuse ice cover and water whenever their backscatter signals are:
    - Equally low—this occurs when the water is calm and the ice is well frozen and thin, purely columnar or bottomfast or melting and wet or overlain by wet snow/puddles.
    - Equally high—this occurs when the water is roughened by wind or flow and the ice is well frozen, thick and impure or melting and very rough.
- Table 1 lists our expectations regarding the utility of alternate approaches—relative to that of radiometric analysis—to overcome the challenges identified.

Table 1. Anticipated utility of image analysis approaches—relative to radiometric analysis—to overcome commonly encountered challenges in terms of ice/water classification. Key: '-' minimal, '-/+' limited, '+' moderate, '++' strong.

	Utility			
Challenge	Polarimetry	Texture	CCD[1)]	BICD[2)]
The classes have equally low backscatters; e.g. calm water, black ice and new ice.	-/+	-/+	-/+	+
The classes have equally high backscatters; e.g. windy water, snow ice and frazil ice.	+	+	++	+

1) Coherent Change Detection; requires InSAR images with suitable time intervals.
2) Backscatter Intensity Change Detection; requires the presence and absence of temporal change in the backscatter of water and ice, respectively.

Acknowledgements

We would like to acknowledge the support from project lead Ghanashyan Ranjitkar of CanmetENERGY-Ottawa, Natural Resources Canada (NRCan). Financial support for our study was received from NRCan's Office of Energy Research and Development. Finally, we would like to thank internal reviewer Naomi Short for her helpful comments and suggestions.

References

Bamler, R. and P. Hartl. (1998). "Synthetic Aperture Radar Interferometry", *Inverse Problems*, Vol. 14, No. 4, pp. R1-R54.

Banks, S.N., D.J. King, A. Merzouki, and J. Duffe. (2014). "Characterizing scattering behaviour and assessing potential for classification of arctic shore and near-shore land covers with Fine Quad-Pol RADARSAT-2 data", *Canadian Journal of Remote Sensing*, Vol. 40, No. 4, pp. 291-314.

Baraldi, A. and F. Parmiggiani. (1995). *An investigation of the textural characteristics associated with Gray Level Co-occurrence Matrix statistical parameters.* 33 edition, 304 p.

Beaton, A., J.J. van der Sanden, K. Corston, A. Deschamps, and S. Tolszczuk-Leclerc. (2017). "Near Real-Time Monitoring of Ice Break-up in the Far North of Ontario Using RADARSAT-2 in Support of Provincial Flood Forecasting and Warning", In: *Proceedings of the 19th Workshop on the Hydraulics of Ice Covered Rivers,* Whitehorse, Yukon, 9-12 July 2017.

Chu, T., A. Das, and K.E. Lindenschmidt. (2015). "Monitoring the Variation in Ice-Cover Characteristics of the Slave River, Canada Using RADARSAT-2 Data—A Case Study", *Remote Sensing*.

Chu, T. and K.E. Lindenschmidt. (2016). "Integration of space-borne and air-borne data in monitoring river ice processes in the Slave River, Canada", *Remote Sensing of Environment*, Vol. 181, pp. 65-81.

Clausi, D.A., A.K. Qin, M.S. Chowdhury, P. Yu, and P. Maillard. (2010). "MAGIC: MAp-Guided Ice Classification System", *Canadian Journal of Remote Sensing*, Vol. 36, No. sup1, pp. S13-S25.

Cloude, S.R. and E. Pottier. (1997). "An entropy based classification scheme for land applications of polarimetric SAR", *IEEE Transactions on Geoscience and Remote Sensing*, Vol. 35, No. 1, pp. 68-78.

Cutler, P.J., W.C. Schwartzkopf, and F.W. Koehler. (2015). "Robust automated thresholding of SAR imagery for open-water detection", In: *Radar Conference (RadarCon),* Arlington, VA, 10-15 May 2015, pp. 0310-0315.

d'Auteuil, S., C. Ridd, E.L. Bibeau, and A.H. Birjandi. (2015). "Riverine hydrokinetic resource assessment and site selection using low cost satellite and aerial winter imagery", In: *Proceedings of the 3rd Marine Energy Technology Symposium (METS 2015),* Washington, D.C., 27-29 April 2015, pp. -4.

Duguay, C.R., M. Bernier, Y. Gauthier, and A. Kouraev. (2015). "Remote sensing of lake and river ice", In: Anonymous. Remote Sensing of the Cryosphere, John Wiley & Sons, Ltd., 1 edition, pp. 274-307.

Flores, M.M., F. Parmiggiani, and L.L. Lopez. (2014). "Automatic measurement of polynya area by anisotropic filtering and Markov random fields", *IEEE Journal of Selected Topics in Applied Earth Observations and Remote Sensing*, Vol. 7, No. 5, pp. 1665-1674.

Freeman, A. and S.L. Durden. (1998). "A three-component scattering model for polarimetric SAR data", *IEEE Transactions on Geoscience and Remote Sensing*, Vol. 36, No. 3, pp. 963-973.

Gagnon, L. and A. Jouan. (1997). "Speckle Filtering of SAR Images - A Comparative Study Between Complex-Wavelet-Based and Standard Filters", In: *Proceedings of SPIE 3169: Wavelet Applications in Signal and Image Processing V,* San Diego, CA, 30 October 1997.

Gauthier, Y., F. Weber, S. Savary, M. Jasek, L.M. Paquet, and M. Bernier. (2006). "A combined classification scheme to characterise river ice from SAR data", *EARSeL eProceedings*, Vol. 5, No. 1, pp. 77-88.

Gauthier, Y., L.M. Paquet, A. Gonzalez, and M. Bernier. (2008). "Using radar images and GIS to support ice-related flood forecasting", *Geomatica*, Vol. 62, No. 2, pp. 139-149.

Gauthier, Y., M. Tremblay, M. Bernier, and C. Furgal. (2010). "Adaptation of a radar-based river ice mapping technology to the Nunavik context", *Canadian Journal of Remote Sensing*, Vol. 36, No. SUPPL., pp. S168-S185.

Geldsetzer, T. and J.J. Yackel. (2009). "Sea ice type and open water discrimination using dual co-polarized C-band SAR", *Canadian Journal of Remote Sensing*, Vol. 35, No. 1, pp. 73-84.

Geldsetzer, T., J.J. van der Sanden, and B. Brisco. (2010). "Monitoring Lake Ice during Spring Melt using RADARSAT-2 SAR", *Canadian Journal of Remote Sensing*, Vol. 36, No. 2, pp. S391-S400.

Geldsetzer, T. and J.J. van der Sanden. (2013). "Identification of polarimetric and nonpolarimetric C-band SAR parameters for application in the monitoring of lake ice freeze-up", *Canadian Journal of Remote Sensing*, Vol. 39, No. 3, pp. 263-275.

Gill, J.P.S. and J.J. Yackel. (2012). "Evaluation of C-band SAR polarimetric parameters for discrimination of first-year sea ice types", *Canadian Journal of Remote Sensing*, Vol. 38, No. 3, pp. 306-323.

Hall, D.K. (1998). "Remote sensing of snow and ice using imaging radar", In: F.M.Henderson & A.J.Lewis (Eds.), Principles and Applications of Imaging Radar*,* New York etc., John Wiley & Sons, Inc., 3rd edition, pp. 677-703.

Haralick, R.M. and W.F. Bryant. (1976). *Documentation of procedures for textural/spatial pattern recognition techniques.* Lawrence, USA, University of Kansas, Remote Sensing Laboratory, 278-1.

IAHR. (1980). *Multilingual Ice Terminology. Addendum I.* Research Centre for Water Resources, Budapest, Hungary, International Association for Hydraulic Research, 24 p.

Kotsiantis, S.B. (2007). "Supervised machine learning: A review of classification techniques", *Informatica*, Vol. 31, No. 3, pp. 249-268.

Krieger, G., M. Zink, M. Bachmann, B. Bräutigam, D. Schulze, M. Martone, P. Rizzoli, U. Steinbrecher, J. Walter Antony, F. De Zan, I. Hajnsek, K. Papathanassiou, F. Kugler, M. Rodriguez Cassola, M. Younis, S. Baumgartner, P. López-Dekker, P. Prats, and A. Moreira. (2013). "TanDEM-X: A radar interferometer with two formation-flying satellites", *Acta Astronautica*, Vol. 89, pp. 83-98.

Lee, J.S., M.R. Grunes, and R. Kwok. (1995). "Classification of multi-look polarimetric SAR imagery based on complex Wishart distribution", *International Journal of Remote Sensing*, Vol. 15, No. 11, pp. 2299-2311.

Lee, J.S. and E. Pottier. (2009). *Polarimetric radar imaging: from basics to applications.* Boca Raton, FL etc., CRC Press, Taylor & Francis Group, 398 p.

Leigh, S., Z. Wang, and D.A. Clausi. (2014). "Automated ice-water classification using dual polarization SAR satellite imagery", *IEEE Transactions on Geoscience and Remote Sensing*, Vol. 52, No. 9, pp. 5529-5539.

Łoś, H., K. Osinska-Skotak, J. Pluto-Kossakowska, M. Bernier, Y. Gauthier, M. Jasek, and A. Roth. (2016). "Comparison of C-band and X-Band polarimetric sar data for river ice classification on the Peace River", In: *Proceedings of the 23rd International Archives of the Photogrammetry, Remote Sensing and Spatial Information Sciences Congress (ISPRS 2016),* Prague, Czech Republic, 12-19 July 2016, Vol. 41, pp. 543-548.

Mermoz, S., S. Allain, M. Bernier, E. Pottier, and I. Gherboudj. (2009). "Classification of river ice using polarimetric SAR data", *Canadian Journal of Remote Sensing*, Vol. 35, No. 5, pp. 460-473.

Moreira,A., Prats-Iraola,P., Younis,M., Krieger,G., Hajnsek,I., & Papathanassiou,K.P. 2013. A Tutorial on Synthetic Aperture Radar. *IEEE Geoscience and Remote Sensing Magazine*, *1,* 6-43.

Natural Resources Canada. (2017). *Microwave Remote Sensing*, Natural Resources Canada*,* http://www.nrcan.gc.ca/node/9371. Last accessed, June 19, 2018.

Ochilov, S. and D.A. Clausi. (2012). "Operational SAR sea-ice image classification", *IEEE Transactions on Geoscience and Remote Sensing*, Vol. 50, No. 11 PART1, pp. 4397-4408.

Qi, Z., A.G.O. Yeh, X. Li, and Z. Lin. (2012). "A novel algorithm for land use and land cover classification using RADARSAT-2 polarimetric SAR data", *Remote Sensing of Environment*, Vol. 118, pp. 21-39.

Richards, J.A. (1993). *Remote sensing digital image analysis. An introduction.* Berlin etc., Springer-Verlag, 2nd edition edition, 340 p.

Rosen, P.A., S. Hensley, I.R. Joughin, F.K. Li, S.N. Madsen, E. Rodriguez, and R.M. Goldstein. (2000). "Synthetic Aperture Radar Interferometry", *Proceedings of the IEEE*, Vol. 88, No. 3, pp. 333-382.

Santoro, M. and U. Wegmuller. (2014). "Multi-temporal Synthetic Aperture Radar Metrics Applied to Map Open Water Bodies", *IEEE Journal of Selected Topics in Applied Earth Observations and Remote Sensing*, Vol. 7, No. 8, pp. 3225-3238.

Shokr, M. (2009). "Compilation of a radar backscatter database of sea ice types and open water using operational analysis of heterogeneous ice regimes", *Canadian Journal of Remote Sensing*, Vol. 35, No. 4, pp. 369-384.

Sobiech, J. and W. Dierking. (2013). "Observing lake- and river-ice decay with SAR: advantages and limitations of the unsupervised k-means classification approach", *Annals of Glaciology*, Vol. 54, No. 62, pp. 65-72.

Thompson, A.A. (2015). "Overview of the RADARSAT Constellation Mission", *Canadian Journal of Remote Sensing*, Vol. 41, No. 5, pp. 401-407.

Touzi, R. (2007). "Target Scattering Decomposition in Terms of Roll-Invariant Target Parameters", *IEEE Transactions on Geoscience and Remote Sensing*, Vol. 45, No. 1, pp. 73-84.

Ullmann, T., S.N. Banks, A. Schmitt, and T. Jagdhuber. (2017). "Scattering characteristics of X-, C- and L-band polsar data examined for the tundra environment of the Tuktoyaktuk Peninsula, Canada", *Applied Sciences*, Vol. 7, No. 6.

Unterschultz, K.D., J.J. van der Sanden, and F.E. Hicks. (2009). "Potential of RADARSAT-1 for the monitoring of river ice: Results of a case study on the Athabasca River at Fort McMurray, Canada", *Cold Regions Science and Technology*, Vol. 55, No. 2, pp. 238-248.

van der Sanden, J.J., H. Drouin, F.E. Hicks, and S. Beltaos. (2009). "Potential of RADARSAT-2 for the Monitoring of River Freeze-up Processes", In: *Proceedings of the 15th Workshop on River Ice,* St.John's, NF, 15-17 June 2009, pp. -14.

van der Sanden, J.J. and H. Drouin. (2011). "Polarimetric RADARSAT-2 for river freeze-up monitoring: preliminary results", In: *Proceedings of the 5th International Workshop on Science and Applications of SAR Polarimetry and Polarimetric Interferometry (SP-695),* Frascati (Rome), Italy, 24-28 January 2011, pp. -8.

van der Sanden, J.J., T. Geldsetzer, N.H. Short, and B. Brisco. (2012). *Advanced SAR Applications for Canada's Cryosphere (Freshwater Ice and Permafrost) - Final Technical Report for the Government Related Initiatives Program (GRIP).* Ottawa, Natural Resources Canada, ESS Contribution Number 20120212, 80 p.

van der Sanden, J.J., H. Drouin, and Y. Bian. (2013). "Repeat Pass InSAR Observations of River and Lake Ice Cover: A Preliminary Evaluation of Information Content", In: *Proceedings of the 17th Workshop on River Ice,* Edmonton, Alberta, 21 - 24 July 2013, pp. 258-271.

van der Sanden, J.J. and T. Geldsetzer. (2015). "Compact Polarimetry in Support of Lake Ice Breakup Monitoring: Anticipating the RADARSAT Constellation Mission", *Canadian Journal of Remote Sensing*, Vol. 41, No. 5, pp. 440-457.

van der Sanden, J.J. and N.H. Short. (2017). "Radar satellites measure ice cover displacements induced by moving vehicles", *Cold Regions Science and Technology*, Vol. 133, No. Supplement C, pp. 56-62.

van der Sanden, J.J., N.H. Short, and H. Drouin. (submitted). "InSAR coherence for automated lake ice extent mapping: TanDEM-X bistatic and pursuit monostatic results", *International Journal of Applied Earth Observation and Geoinformation*.

Wendleder, A., B. Wessel, A. Roth, M. Breunig, K. Martin, and S. Wagenbrenner. (2013). "TanDEM-X water indication mask: Generation and first evaluation results", *IEEE Journal of Selected Topics in Applied Earth Observations and Remote Sensing*, Vol. 6, No. 1, pp. 171-179.

Woodhouse, I.H. (2006). *Introduction to Microwave Remote Sensing.* Boca Raton, Florida, CRC Press, Taylor & Francis Group, 370 p.

Xu, R. and D. Wunsch. (2005). "Survey of clustering algorithms", *IEEE Transactions on Neural Networks*, Vol. 16, No. 3, pp. 645-678.

Yamaguchi, Y., T. Moriyama, M. Ishido, and H. Yamada. (2005). "Four-component scattering model for polarimetric SAR image decomposition", *IEEE Transactions on Geoscience and Remote Sensing*, Vol. 43, No. 8, pp. 1699-1706.

Yitayew, T.G., A.P. Doulgeris, T. Eltoft, W. Dierking, C. Brekke, and A. Rõsel. (2017). "Sea ice segmentation using Tandem-X pursuit monostatic and alternative bistatic modes", In: *Proceedings of the 2017 IEEE International Geoscience and Remote Sensing Symposium (IGARSS): International Cooperation for Global Awareness,* Fort Worth, Texas, 23-28 July 2017, pp. 334-337.

Yu, P., A.K. Qin, and D.A. Clausi. (2012a). "Feature extraction of dual-pol SAR imagery for sea ice image segmentation", *Canadian Journal of Remote Sensing*, Vol. 38, No. 3, pp. 352-366.

Yu, P., A.K. Qin, and D.A. Clausi. (2012b). "Unsupervised Polarimetric SAR Image Segmentation and Classification Using Region Growing With Edge Penalty", *IEEE Transactions on Geoscience and Remote Sensing*, Vol. 50, No. 4, pp. 1302-1317.

Zakhvatkina, N., V.Y. Alexandrov, O.M. Johannessen, S. Sandven, and I.Y. Frolov. (2013). "Classification of sea ice types in ENVISAT synthetic aperture radar images", *IEEE Transactions on Geoscience and Remote Sensing*, Vol. 51, No. 5, pp. 2587-2600.

Zakhvatkina, N., A. Korosov, S. Muckenhuber, S. Sandven, and M. Babiker. (2017). "Operational algorithm for ice-water classification on dual-polarized RADARSAT-2 images", *The Cryosphere*, Vol. 11, No. 1, pp. 33-46.